



OPEN

Copper oxides supported sulfur-doped porous carbon material as a remarkable catalyst for reduction of aromatic nitro compounds

Marzie Amirjan, Firouzeh Nemati[✉], Zeinab Elahimehr & Yalda Rangraz

Synthesis and manufacturing of metal–organic framework derived carbon/metal oxide nanomaterials with an advisable porous structure and composition are essential as catalysts in various organic transformation processes for the preparation of environmentally friendly catalysts. In this work, we report a scalable synthesis of sulfur-doped porous carbon-containing copper oxide nanoparticles (marked $\text{Cu}_x\text{O}@CS-400$) via direct pyrolysis of a mixture of metal–organic framework precursor called HKUST-1 and diphenyl disulfide for aromatic nitro compounds reduction. X-ray diffraction, surface area analysis (BET), X-ray energy diffraction (EDX) spectroscopy, thermal gravimetric analysis, elemental mapping, infrared spectroscopy (FT-IR), transmission electron microscope, and scanning electron microscope (FE-SEM) analysis were accomplished to acknowledge and investigate the effect of S and Cu_xO as active sites in heterogeneous catalyst to perform the reduction-nitro aromatic compounds reaction in the presence of $\text{Cu}_x\text{O}@CS-400$ as an effective heterogeneous catalyst. The studies showed that doping sulfur in the resulting carbon/metal oxide substrate increased the catalytic activity compared to the material without sulfur doping.

Heterogeneous catalysts are one of the strategic designs of chemical research in the industrial manufacturing of many fine chemicals due to their recyclability^{1–7}. In recent decades, disparate species of heterogeneous catalysts have been developed and used. Among them, porous carbon/metal oxide materials have attracted considerable interest as extraordinary catalysts because of their innate structural attributes such as thermal stability, high surface area, adjustable porous structure, and beneficial mechanical properties^{7–12}. However, the porous carbon-based catalysts, due to the inherent inertia of the surface chemistry of the genuine carbon materials, have suffered from special restrictions on morphology, specific surface area, and size controls, which have limited their catalytic applications^{2,8,10,12–14}.

Accordingly, researchers in recent decades, in order to solve the above problems, have used heteroatoms doping into a porous carbon matrix and carbon framework that can present completely different catalytic properties^{5,15–18}. Thus, specifically, non-metal heteroatoms (such as B, N, S, P, and halogen) are doped into the sp^2 lattice of graphitic carbon. As a result, the distinction in electronegativity between carbon and heteroatoms causes them to adjust their optoelectronic and chemical properties^{15,17,19–21}. Hence, heteroatoms, depending on their chemical configuration in the carbon matrix, can increase the interaction between the metal species and the support and lead to the production of new catalytic active sites, which is beneficial for the enhancement of catalytic reactivity in organic reactions^{5,14,22–25}. Among different heteroatoms, the doping of sulfur is similar to that of nitrogen, and in some cases, it has a better catalytic conclusion. In comparison to nitrogen, due to the larger covalent radius of sulfur, the presence of a sulfur atom (atomic size = 102 pm) inside the carbon lattice can significantly raise the interlayer space in the carbon network. So, enlarging the interlayer distance in carbon network by doping heteroatoms with large-radius is an effective approach that significantly increases the basic sites, promoting the adsorption of organic compounds^{15–17,26,27}.

Thus, it is critical to use a sensible design and the right synthesis method to produce heteroatom-doped porous carbon/metal oxide-based catalysts with two essential characteristics: a regular porous structure and a large specific surface area^{9,27–33}. Since they combine metal ions (or metal categories) with organic linkers,

Department of Chemistry, Semnan University, Semnan 35131-19111, Iran. ✉email: fnemati@semnan.ac.ir

metal–organic frameworks (MOFs), also known as porous coordination and polymers (PCPs), have garnered a lot of attention. These features include an ordered porous structure, a large specific surface area, high-grade electrical conductance, adjustable porosity, an adjustable numerical structure, and superior resistance to heat and chemicals^{30,31,34,35}. Therefore, MOFs have emerged as a category of promising precursors for synthesizing carbon-based materials via different temperatures of pyrolysis^{17,25,31,36}. This synthesis strategy of carbon substrates derived from MOFs can not only increase metal loading and thus the number of catalytic active sites such as Cu_xO , but also furnish a homogenous dispensation of heteroatoms, metals, and metal oxides inside the pores of carbon-based materials^{15,17,20,37,38}. As a result, porous carbon/metal oxide materials derived from MOFs effectively maintain the pore construction and large specific surface area of MOF precursors and generally have lower densities, more exposed active sites like Cu_xO , and higher stability, thereby maximizing their performance^{10,14,15,38–42}.

for the first time, copper oxides/sulfur doped carbon-based catalyst (denoted as $\text{Cu}_x\text{O}@CS-400$) have been synthesized with different ratios of diphenyl disulfide as sulfur and carbon source, using HKUST-1 as a precursor under an inert atmosphere and moderate-temperature pyrolysis conditions, and the nitro aromatic reduction was used to gauge its effectiveness. We have devised a successful method for converting unstable HKUST-1 into stable organic framework materials using the decarboxylation reaction under mild annealing conditions. During this process, the fragile coordination bonds in HKUST-1 were replaced with stable covalent C–C bonds, which show better catalytic properties from the parent MOF. Furthermore, in situ sulfur doping improves the material's properties.

In continuation of our antecedent researches and studies in the field of synthesis and design of the novel heterogeneous catalysts^{1,2,43,44}, and also their application in various synthesis reactions including the reduction of nitroaromatic compounds^{1,2,44–46}, in this article, we have synthesized sulfur-doped porous carbon/copper oxides-based catalyst (denoted as $\text{Cu}_x\text{O}@CS-400$) with different ratios of sulfur using HKUST-1 as a precursor under an inert atmosphere at moderate-temperature pyrolysis conditions, which $\text{Cu}_x\text{O}@CS-400$ catalyst demonstrated desirable catalytic activity in the reaction of nitroaromatic compounds and its derivatives with NaBH_4 as a reducing factor in very short reaction times and high yields. The general synthesis cycle of the catalyst is illustrated in Figure 1, and details of the laboratory process are described in the experimental department. Briefly, at first, HKUST-1 was synthesized according to the articles. HKUST-1 is a cononant polymer composed of copper ions and 1,3,5-benzentricarboxylate (BTC) ligands, with a special character area of more than $1021.2 \text{ m}^2/\text{g}$. Eventually, $\text{Cu}_x\text{O}@CS-400$ was drafted by moderate-warmth pyrolysis of the admixture of sulfur-doped porous carbons (which was outsourced from HKUST-1) and diphenyl disulfide.

Experimental section

Chemicals

All chemicals used in the synthesis of $\text{Cu}_x\text{O}@CS-400$ and reduction reactions were purchased from Sigma-Aldrich. And reagents and solvents were used directly without renewed refinement.

Devices

Identifying organic and inorganic materials was accomplished by the Furrier Transform Infrared Spectroscopy (FT-IR, 8400S). The X-ray diffraction (XRD, Bruker D8-ADVANCE diffractometer: $\text{Cu}/\text{K}\alpha$ ($\lambda = 0.15406 \text{ nm}$)) was utilized to analyze the crystal structure of solid specimens. The elemental combination and homogeneous dispensation of instances were distinguished via energy-dispersive X-ray (EDX) and elemental mapping procedures. The morphology and structural attributes of the specimens were appraised per the passing electron

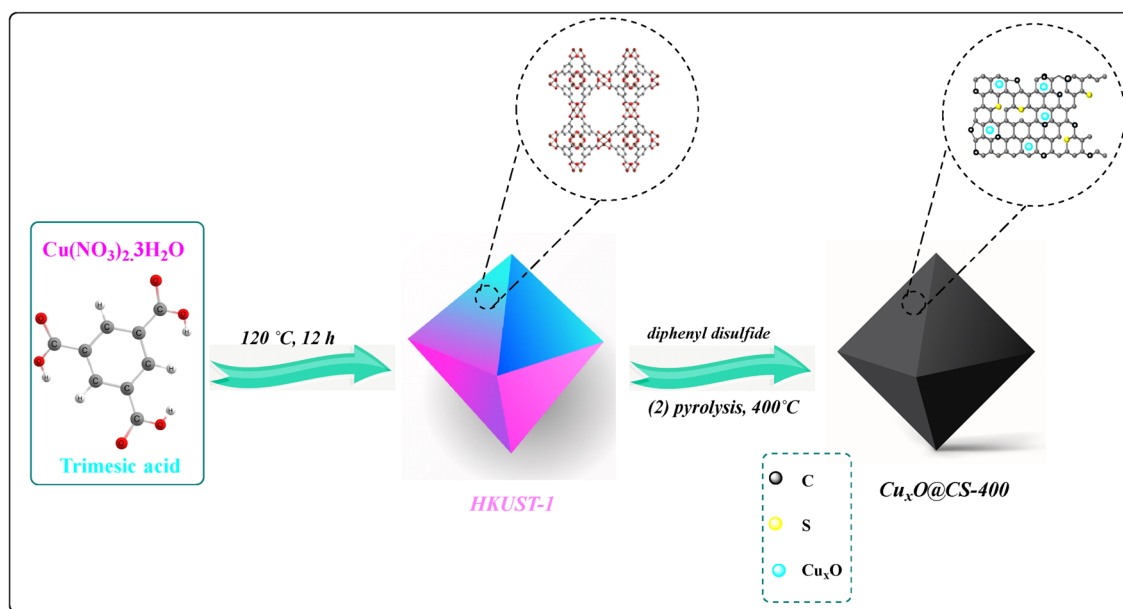


Figure 1. Schematic Pathway of synthesis of $\text{Cu}_x\text{O}@CS-400$.

microscope or magnifier (TEM, Philips EM208S 100 kV) and scanning electron microscope (FE-SEM, TESCAN MIRA3). The Brauer–Emmett–Teller (BET) analysis for the measurement of the specific area and porosity distribution of the solid sample was provided at a low temperature (150 °C) via N₂ adsorption–desorption isotherms (Belsorp Mini II).

The procedure for the synthesis of, porous carbon/copper oxides catalyst derived from MOFs

Synthesis of HKUST-1

HKUST-1 was synthesized from copper (II) nitrate trihydrate (Cu(NO₃)₂·3H₂O) and 1,3,5-benzenetricarboxylic acid (C₉H₆O₆) based upon the reported methodology⁴⁷. Specifically, Cu(NO₃)₂·3H₂O (2.174 g, 8.998 mmol) was dissolved in 30 mL distilled water; in the meantime, benzene-1,3,5-tricarboxylic acid (1.05 g, 4996 mmol) as an organic ligand was dissolved in 30 mL ethanol. Subsequently, the solutions were blended together and transferred to a 100 mL round bottom flask, and the mixture was continuously agitated for 30 min under an intense stirring situation at ambient temperature. After stirring for 30 min, the mixture was transferred to a 100 mL Teflon-lined stainless-steel autoclave and kept at 120 °C for 12 h. Eventually, after cooling to room temperature, the blue powder was collected by centrifugation, and washed several times with deionized water and ethanol alternately, and dried at 60 °C in a vacuum for 12 h, to modify the synthesized HKUST-1, the obtained blue powder was chemically purified with ethanol and dichloromethane, and finally, in order to remove solvent molecules and activate the synthesized HKUST-1, the solid powder was heated in an oven at 150 °C for 12 h.

Synthesis of Cu_xO@CS-400

The activated MOF powder (HKUST-1) and Diphenyl disulfide at different ratios (H:D 1:2, 1:3, and 1:5) were dissolved in 15 mL of *N,N*-dimethylformamide. The mixture was stirred for 24 h and dried in an oven at 60 °C. The precursor prepared was carbonized straight under the nitrogen atmosphere at 400 °C for 2 h with a thermal rapidity of 10 °C min⁻¹ under the N₂ atmosphere. Finally, the above-carbonized sample was labeled Cu_xO@CS-400 and was used as a catalyst with excellent efficiency in organic reactions, and as expected, the catalyst has significant recyclability and can run eight times without any obvious decline in catalytic activity. Figure 1 epitomizes the schematic representation of the synthesis methodology of the carbon-based copper oxide catalyst. The Cu_xO@C-400 was synthesized accordingly, without diphenyl disulfide.

Catalytic test

1 mmol of substrate, 3 mL of deionized water and 7 mg of Cu_xO@CS-400 were stirred for a few minutes at ambient temperature. Following, NaBH₄ (2 mmol) as the reductant was added to the above mixture, and the reaction mixture was stirred at 55 °C. The progression of the hydrogenation reaction was followed by TLC. At the end of the reaction time, the Cu_xO@CS-400 was separated, rinsed, and reused. The catalyst was isolated, the resultant catalyst-free mixture was extracted by EtOAc as an organic phase (3 × 5 mL). The organic (EtOAc) layer was separated and dried by sodium sulphate. Eventually, by vaporizing the solvent, the pure product was gained (Table 1).

Some spectra data

Aniline (Table 1, entry 1), light yellow liquid, ¹H NMR (300 MHz, CD₃Cl) δ: 7.12 (t, *J* = 7.8 Hz, 2H), 6.70 (t, *J* = 7.2 Hz, 1H), 6.62 (d, *J* = 7.5 Hz, 2H), 3.41 (br s, 2H).

4-Aminobenzonitrile (Table 1, entry 2) White powder, M.P. 85 °C, ¹H NMR (300 MHz, CD₃Cl) δ: 7.39 (d, *J* = 7.8 Hz, 2H), 6.65 (d, *J* = 7.5 Hz, 2H), 3.5 (br s, 2H).

4-Bromo aniline (Table 1, entry 3) White powder, M.P. 65–66 °C, ¹H NMR (300 MHz, CD₃Cl) δ: 7.21 (d, *J* = 8.2 Hz, 2H), 6.54 (d, *J* = 8.4 Hz, 2H), 3.78 (br s, 2H).

4-Chloro-2-trifluoromethyl aniline (Table 1, entry 4), Pinkish crystal, M.P.: 35–38 °C, ¹H NMR (300 MHz, CD₃Cl) δ: 7.39 (s, 1H), 7.23 (d, *J* = 8.5 Hz, 1H), 6.62 (d, *J* = 8.7 Hz, 1H), 3.99 (br s, 2H).

o-Phenylenediamine (Table 1, entry 5), Yellowish crystal, M.P.: 101–103 °C, ¹H NMR (300 MHz, CD₃Cl) δ: 6.68 (m, 4H), 3.31 (br s, 2H).

4-Aminophenol (Table 1, entry 8) Light brown powder, M.P.: 185–189 °C, ¹H NMR (300 MHz, CD₃Cl) δ: 8.42 (br s, 1H), 6.4–6.49 (m, 4H), 4.32 (br s, 2H).

4-Aminobenzaldehyde (Table 1, entry 9) Slight yellow crystal, M.P.: 68–71 °C, ¹H NMR (300 MHz, CD₃Cl) δ: 9.76 (s, 1H), 7.57 (d, *J* = 8.4 Hz, 2H), 6.65 (d, *J* = 8.1 Hz, 2H), 4.85 (br s, 2H).

Results and discussion

Preparation of Cu_xO@CS-400

Figure 1 illustrates the process to prepare Cu_xO@CS-400 catalyst, which was synthesized by thermal pyrolysis of a mixture of HKUST-1 and diphenyl disulfide at 400 °C for 2 h. As shown in Figure 1, firstly, the HKUST-1 was constructed according to the literature⁴⁷. In the second step, the sulfur heteroatom was infiltrated into porous HKUST-1 by thermally annealing the precursor, which had been prepared by the wet-impregnation technique of a mixture of Ph₂S₂ and HKUST-1 in three ratios. After carbonization of the pre-materials in a stationary atmosphere, further organic connections were thermally transmuted into a porous carbon matrix, and Cu_xO@CS-400 was constructed as a heterogeneous catalyst.

Characterization of HKUST-1 and Cu_xO@CS-400

FT-IR analysis

In order to explain the architecture of the Cu_xO@CS-400–2 catalyst, the FT-IR spectrometric study was carried out. In Fig. 2, the FT-IR spectrum of HKUST-1 is presented. Peaks related to C=O asymmetric and symmetric

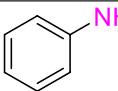
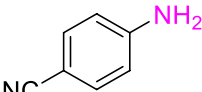
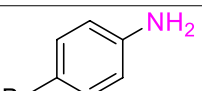
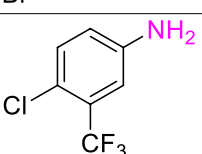
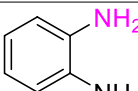
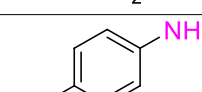
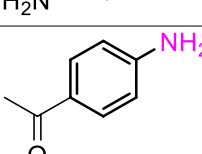
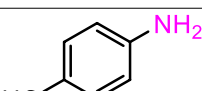
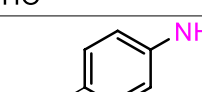
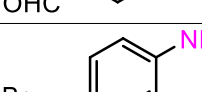
Entry	product	Time (min)	Yield (%)	TOF ^c (mol g ⁻¹ h ⁻¹)	TON ^d
1		35	99	3763	131705
2		45	99	3712	167,040
3		35	99	6951	243,285
4		60	99	4609	276,540
5		30	98	6355	190,650
6		20	100	7724	154,480
7		50	98	3784	189,200
8		25	98	7007	175,175
9		35	96	3411	119,385
10		40	99	7099	283,960

Table 1. Hydrogenation of diverse nitroarenes on Cu_xO@CS-400 subject optimum conditions: ^{a, b} Reaction condition: substrate (1 mmol), NaBH₄ (2 mmol), H₂O (3 mL), Cu_xO@CS-400 (7 mg). ^b Isolated yield. ^c TOF = $\frac{\text{mol of converted substrate}}{\text{mol of catalyst} \times \text{reaction time (h)}} \times 100$. ^d TON = $\frac{\text{yield of product}}{\text{mol of copper in catalyst}}$

stretching vibrations of carboxylic ligands appeared in 1646 cm⁻¹ and 1375 cm⁻¹. The C=C groups of the aromatic rings were observed at 1431 cm⁻¹, which demonstrated that HKUST-1 has been successfully synthesized^{47,48}. On the other hand, obviously, the XRD analysis confirmed the prosperous preparation of HKUST-1. After the pyrolysis of the precursor, due to the production of carbonaceous material, the intensity of C=O was decreased by a considerable amount, and some peaks appeared in the distinctness of 1100–1200 cm⁻¹, which was associated with the C–O and C–S bonds in the as-synthesized Cu_xO@CS-400 catalyst.

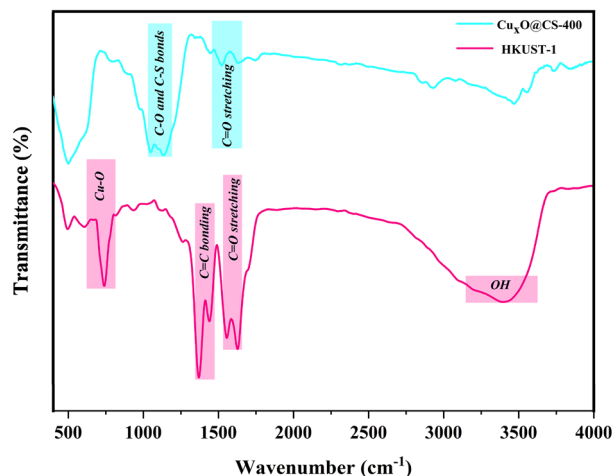


Figure 2. The FT-IR spectra HKUST-1 and $\text{Cu}_x\text{O}@CS-400$ catalyst.

XRD measurement

The crystallinity, phase behavior, and diffraction peaks of HKUST-1 and $\text{Cu}_x\text{O}@CS-400$ materials at different ratios (H: D 1:2, 1:3, and 1:5) were recognized by XRD analysis, as depicted in Fig. 3 and 4. The XRD diffraction peaks of HKUST completely matched with literature reports⁴⁷. After pyrolysis the crystalline nature of the HKUST-1 has changed and new peaks have been created as follow: the as-prepared catalysts exhibited a broad peak at $2\theta = 20\text{--}30^\circ$, which is attributed to the carbon amorphous part of the as-synthesized samples (Fig. 4A–C is the XRD image of $\text{Cu}_x\text{O}@CS-400$ material). Matching to the JCPDS standard card, the peaks at (002) (200) (220), and (113) crystal planes are the diffraction peaks of CuO (JCPDS: 48–1548), and the peaks appearing at (111) and (113) crystal planes in Fig. 4 belong to the diffraction peaks of Cu_2O (JCPDS: 05–0667), which were clearly and precisely indicated in the XRD schemes of the samples⁴⁹. It is noteworthy that the Bragg diffraction peaks of all oxides have a low vehemence, informing that Cu_xO indicates negligible crystallinity with a small granule scale of 34 nm.

For samples in Fig. 4A–C, the characterization results show a transient shift in the refraction summit circumstances and relative intensities. These are caused by varying copper oxide loading ratios in the final materials as a result of varying HKUST-1 and diphenyl disulfide ratios used as precursor materials for sulfur doping in catalyst structures.

The sample with a ratio of 1:2 (H:D) was chosen as the required catalyst, and the subsequent analyses were carried out on it since the catalytic activity of the three manufactured samples (with varying ratios of diphenyl disulfide) had the same catalytic activity.

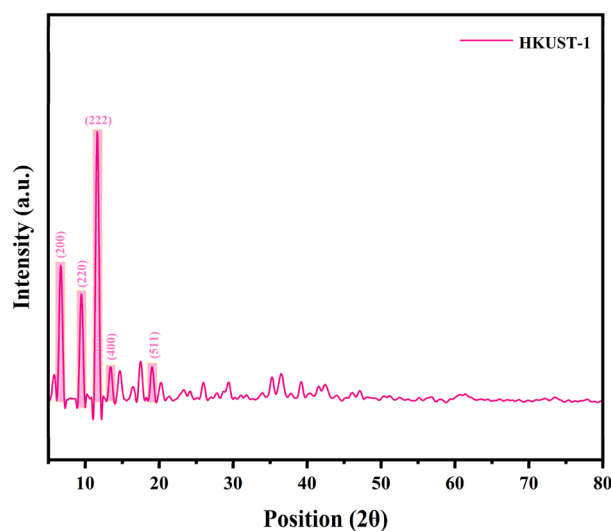


Figure 3. The XRD pattern of HKUST-1.

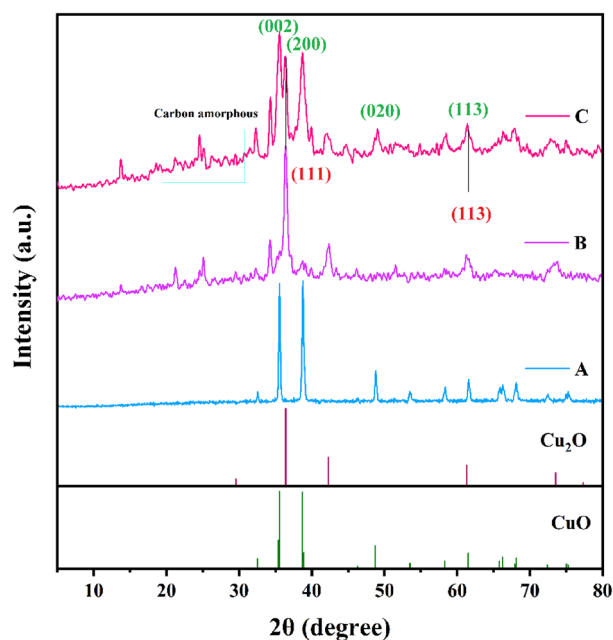
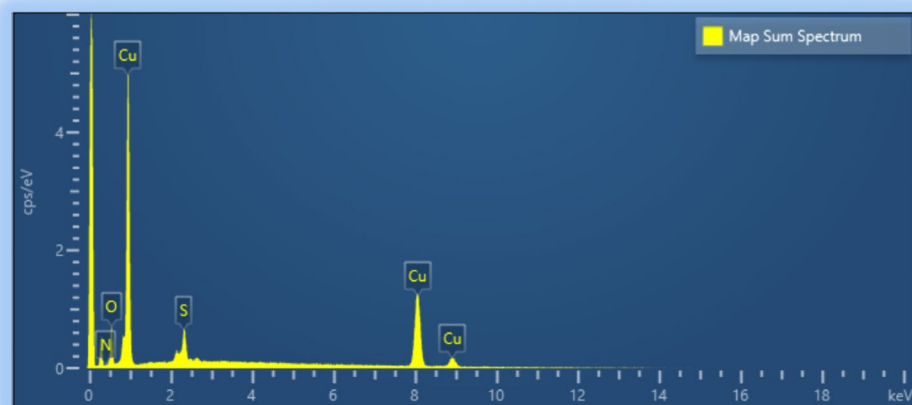


Figure 4. The XRD patterns of $\text{Cu}_x\text{O}@CS-400$ with ratio (H:D 1:5) (A), $\text{Cu}_x\text{O}@CS-400$ with ratio (H:D 1:3) (B), and $\text{Cu}_x\text{O}@CS-400$ with ratio (H:D 1:2) (C).

EDX analysis

The elemental composition of $\text{Cu}_x\text{O}@CS-400$ was studied using EDX analysis, and the results manifested that copper, carbon, oxygen, and sulfur are presented in the particular selected area of the catalyst. This is a verification of the prosperous synthesis of the desired catalyst with high purity (Fig. 5). Moreover, the exact loading of copper in $\text{Cu}_x\text{O}@CS-400$ using the AAS (atomic absorption spectroscopy) technique was found to be 65.5%,



Map Sum Spectrum				
Element	Line Type	Weight %	Weight % Sigma	Atomic %
Cu	L series	65.51	0.76	29.79
O	L series	10.56	0.33	19.07
C	L series	19.47	0.73	46.85
S	L series	4.22	0.17	3.80
N	L series	0.24	0.66	0.49
Total		100.00		100.00

Figure 5. EDX data of $\text{Cu}_x\text{O}@CS-400$.

which increased upon pyrolysis of pre-material in the N_2 atmosphere in comparison with HKUST-1. In addition, the amount of copper is in agreement with the EDX analysis.

Elemental mapping images of $Cu_xO@CS-400$ are shown in Fig. 6, which obviously shows a homogeneous distribution of the desired elements Cu, C, O, especially S, in the structure of the catalyst.

Thermogravimetric analysis

Thermal gravimetric analysis data at HKUST-1 and $Cu_xO@CS-400$ were measured under the air with the heating speed of $10\text{ }^\circ\text{C min}^{-1}$, and outcomes are shown in Fig. 7. The HKUST-1 exhibited three weight loss stages. Two primary degradations, nearly 22 and 19%, befell at $30\text{--}400\text{ }^\circ\text{C}$ and were ascribed to the evaporation of organic solvents inside the pores, either adsorbed or coordinated water. The second degradation was observed from $400\text{ to }550\text{ }^\circ\text{C}$, nearly 60%, owing to the destruction of the HKUST-1 framework⁴⁷. The TGA and DGA analysis of prepared $Cu_xO@CS-400$ concluded that the catalyst exhibited three weight loss stages. Two primary degradations within $50\text{--}450\text{ }^\circ\text{C}$ with weight-loss about 4% and 6.75% was due to the loss of adsorbed water as well as the coordinated water molecules in the carbon substrate. The third destruction was coupled with a weight-loss about 10.23% between $450\text{ and }750\text{ }^\circ\text{C}$ suggesting that residue organic substances has started to decompose and produce some volatiles materials at $450\text{ }^\circ\text{C}$.

The TGA and DTG analyses of prepared $Cu_xO@CS-400$ concluded that the catalyst is stable up to $750\text{ }^\circ\text{C}$ without any significant weight loss (Fig. 7), which lays a solid foundation for convenient catalytic high temperature synthesis reactions.

FE-SEM and TEM analysis

Figure 8 exhibits the scanning electron microscopy (FE-SEM) images of HKUST-1 and $Cu_xO@CS-400$. The FESEM image of HKUST-1 shows a octahedral shaped morphology, as previously reported in the literature⁴⁷. Upon incorporation of diphenyl disulfide and annealing of the pre-material at $400\text{ }^\circ\text{C}$, the structure of HKUST-1 is partially maintained and presents a rough surface due to the decoration of a number of Cu_xO nanoparticles and holes that are produced during the carbonization process.

The structural examination was then assessed in depth using TEM measurements. The scattered Cu_xO nanoparticles enclosed in the carbonaceous matrix are plainly visible in the concentrated black region. The porous carbon matrix that encircles the framework of dense metal oxides is indicated by the lighter portion of the catalyst (Fig. 9).

N_2 adsorption–desorption isotherm

According to IUPAC, the N_2 adsorption–desorption isotherms of HKUST-1 and catalyst belonged to type IV isotherms, with the H_1 hysteresis loop within the relative pressure of $0.1\text{--}0.95$ as presented in Fig. 10. The specific surface areas of HKUST-1 and as-synthesized catalyst were 1021.2 and $2.4221\text{ m}^2/\text{g}$, respectively. It may be due to the agglomeration of Cu_xO nanoparticles during the pyrolysis. The pore size was mainly distributed at 0.4173 and $0.01067\text{ m}^3/\text{g}$ indicating a mesoporous structure. Finally, the average pore size of the catalysts (with different ratios of diphenyl disulfide) was calculated as 1.6345 and 26.826 nm , respectively.

Catalytic performance of $Cu_xO@CS-400$ in the nitroarenes hydrogenation

To better understand the catalytic efficacy of $Cu_xO@CS-400$ nano-catalyst, the 4-nitro aniline has been selected as a catalytic model and subjected to reduction of the nitro aromatic compound in the presence of $NaBH_4$. In order to check the progress of the reaction after the supplementation of the reaction, soft stratum chromatography

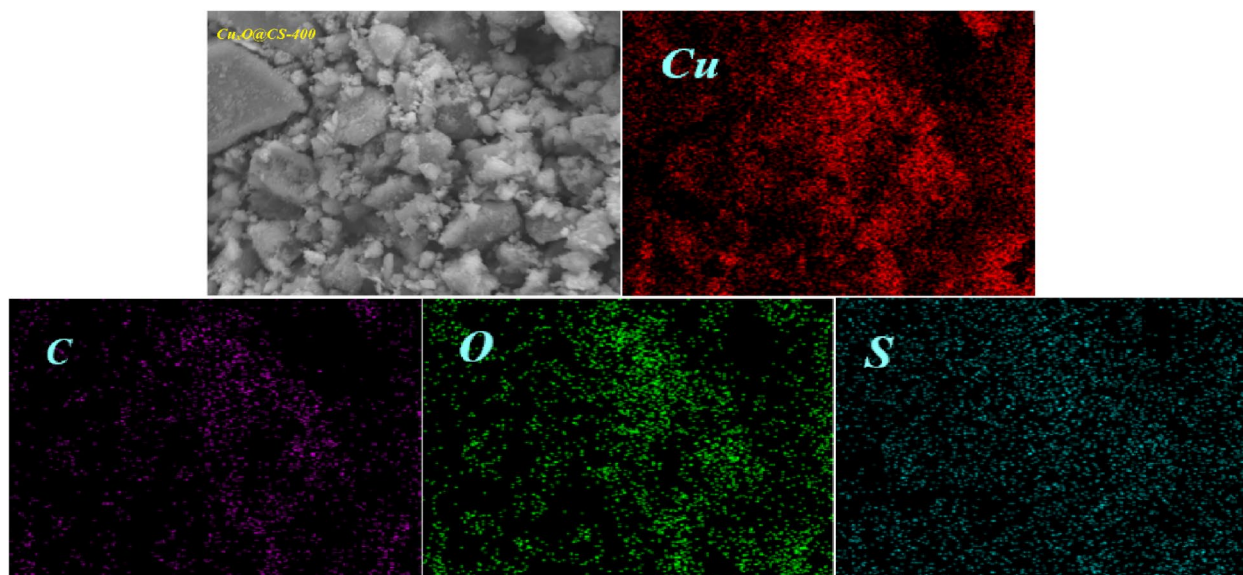


Figure 6. Elemental mapping images of $Cu_xO@CS-400$ for Cu, C, N, O, and S elements.

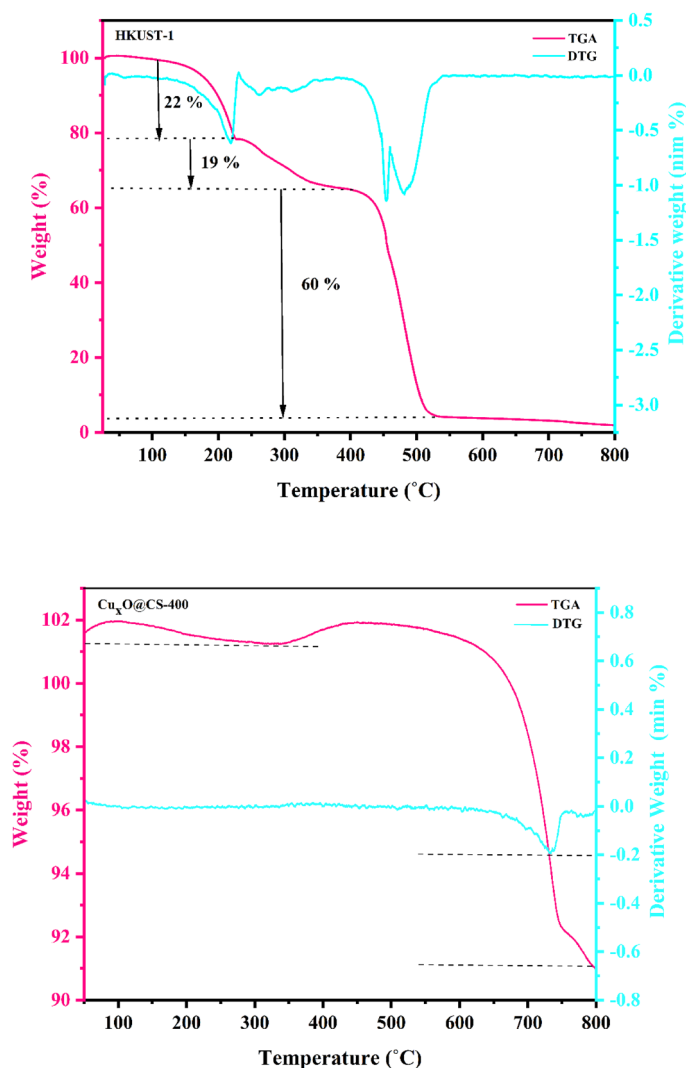


Figure 7. The thermogravimetric curves of HKUST-1 and $\text{Cu}_x\text{O}@CS-400$ catalyst.

(TLC) was performed. Different reaction parameters, including the solvent, the reaction temperature, dosage of the catalyst, and the reductant, were optimized. The reaction consequences are exhibited in Table 1.

Among the examined solvents (entries 8, 9, 10, and 11), the best conversion is obtained in the presence of H_2O (entry 6, 100% conversion). According to a literature review, the presence of water molecules has a significant impact on the conversion of 4-nitro aniline to 1,4-diaminobenzene⁵⁰. The reducing agent screening and its amount show that NaBH_4 is present for the optimal conversion (entry 6). Higher or lower values of the reducing agent result in a reduction in the reaction yield (entries 12–14). Additionally, the impact of reaction temperature was examined (entries 12). The ideal temperature was determined to be 55 °C for the process. The ideal amount of catalyst for the reduction of 4-nitro aniline in the studied process was found to be 7 mg, or 0.072 mol% Cu, based on catalyst screening (entry 6). It should be noted that the reaction stops and no yield is produced in the absence of a catalyst (entry 1). Additionally, the decreased catalytic activity of $\text{Cu}_x\text{O}@C-400$ and HKUST-1 in the absence of the heteroatom demonstrated the critical role that sulphur and copper oxides played in the reaction's progression and final product yield (entries 3 and 4). Furthermore, while employing the sulfur-doped carbon substrate as the catalyst, no product was seen (entry 2).

The catalytic activity of $\text{Cu}_x\text{O}@CS-400$ is examined in relation to other reactants. Different types of substituents on nitro aromatic compounds were transferred to aromatic amines under optimal reaction conditions.

In order to investigate the generality of the transformation, different types of aromatic nitro compounds, derivatives containing electron-donating (OMe, OH, NH_2) and electron-withdrawing (Br, CF_3 , Cl, CN) were reduced under the optimized reaction terms. The supreme returns of the obtained aromatic amines in a very short reaction time indicate the good efficiency of the catalyst in both electron-poor and electron rich substituted nitro aromatic compounds (Table 2). Unfortunately, the yields of the corresponding reduced products were low for aliphatic nitro compounds.

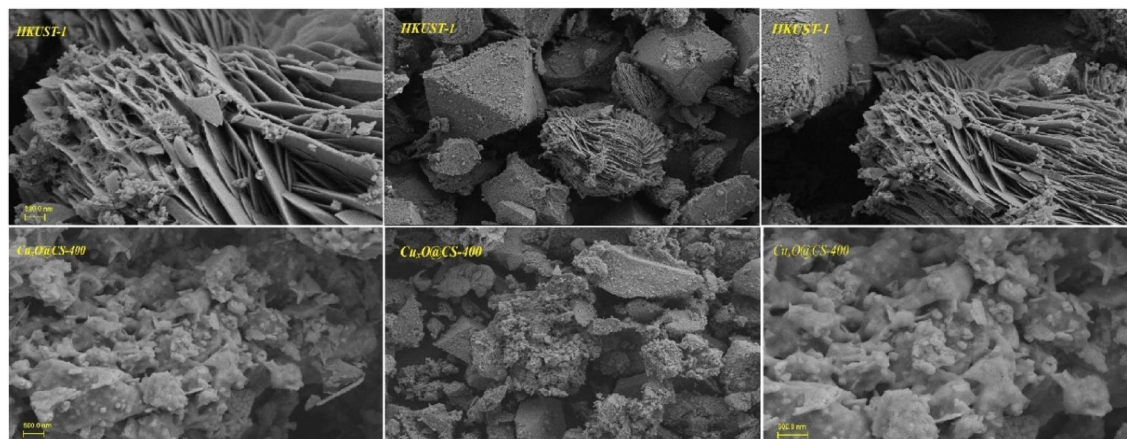


Figure 8. The FE-SEM images of HKUST-1 and $\text{Cu}_x\text{O}@CS-400$ catalyst in different magnifications.

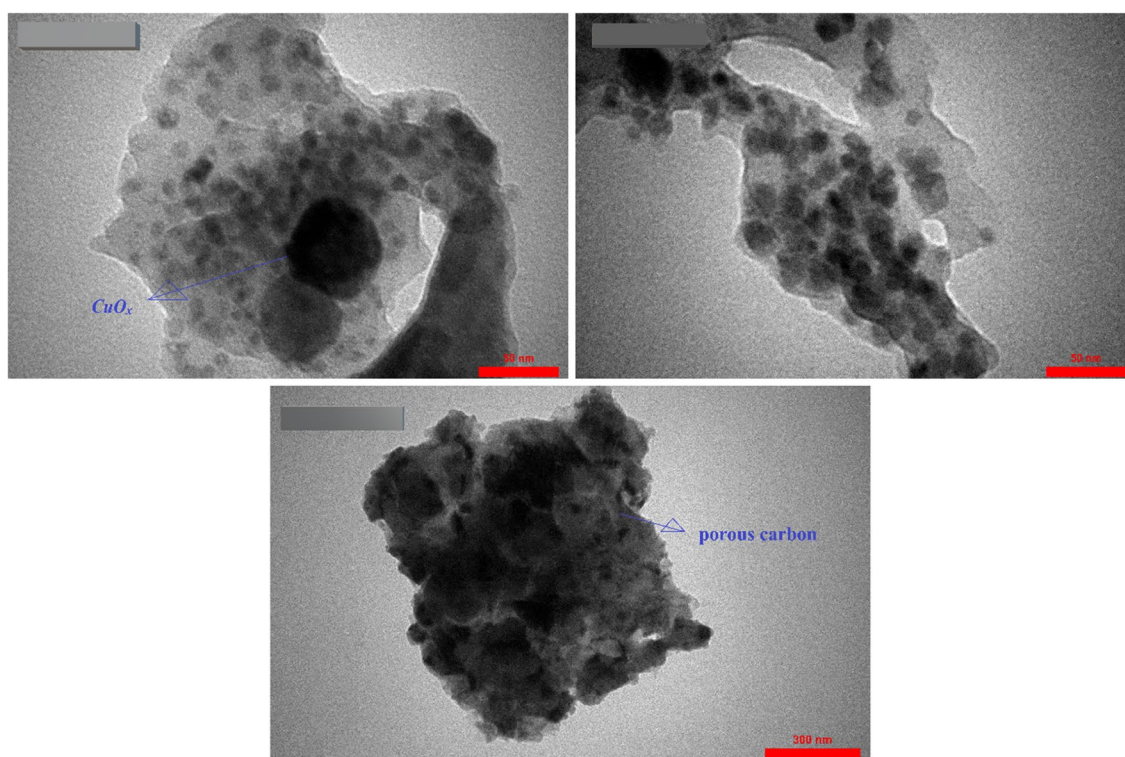


Figure 9. TEM images of $\text{Cu}_x\text{O}@CS-400$ catalyst.

For a more detailed investigation of the catalytic activity of $\text{Cu}_x\text{O}@CS-400$ nano-catalyst, the investigated reaction was performed in the presence of 10 mmol of 4-nitro aniline under optimal reaction conditions, and the yield of the product was reported to be 95%.

Mechanistic sight for the hydrogenation of the nitroarenes by $\text{Cu}_x\text{O}@CS-400$

According to the previous papers⁴³, the plausible mechanistic pathway of the hydrogenation process of nitrobenzene was presented (Fig. 11). Firstly, the reaction between the reducing agent (NaBH_4) and the solvent (H_2O) can generate hydrogen (H_2), which moved to the surface of the catalyst and the catalyst surface activation was done while NaBO_2 was formed as the by-product at room temperature. In the next step, the adsorption of the substrate onto the activated $\text{Cu}_x\text{O}@CS-400$ surface was done to transfer the hydride from the catalyst to the nitrobenzene. Then the nitro reduction was happened and the nitroso group was produced. Subsequently, the hydroxylamine was generated according to the addition reductive process on nitroso group. In final step, the primary amine was released from the surface of the catalyst by hydrogenation of the hydroxylamine and the also the $\text{Cu}_x\text{O}@CS-400$ surface was set-free and for the next hydrogenation catalytic runs.

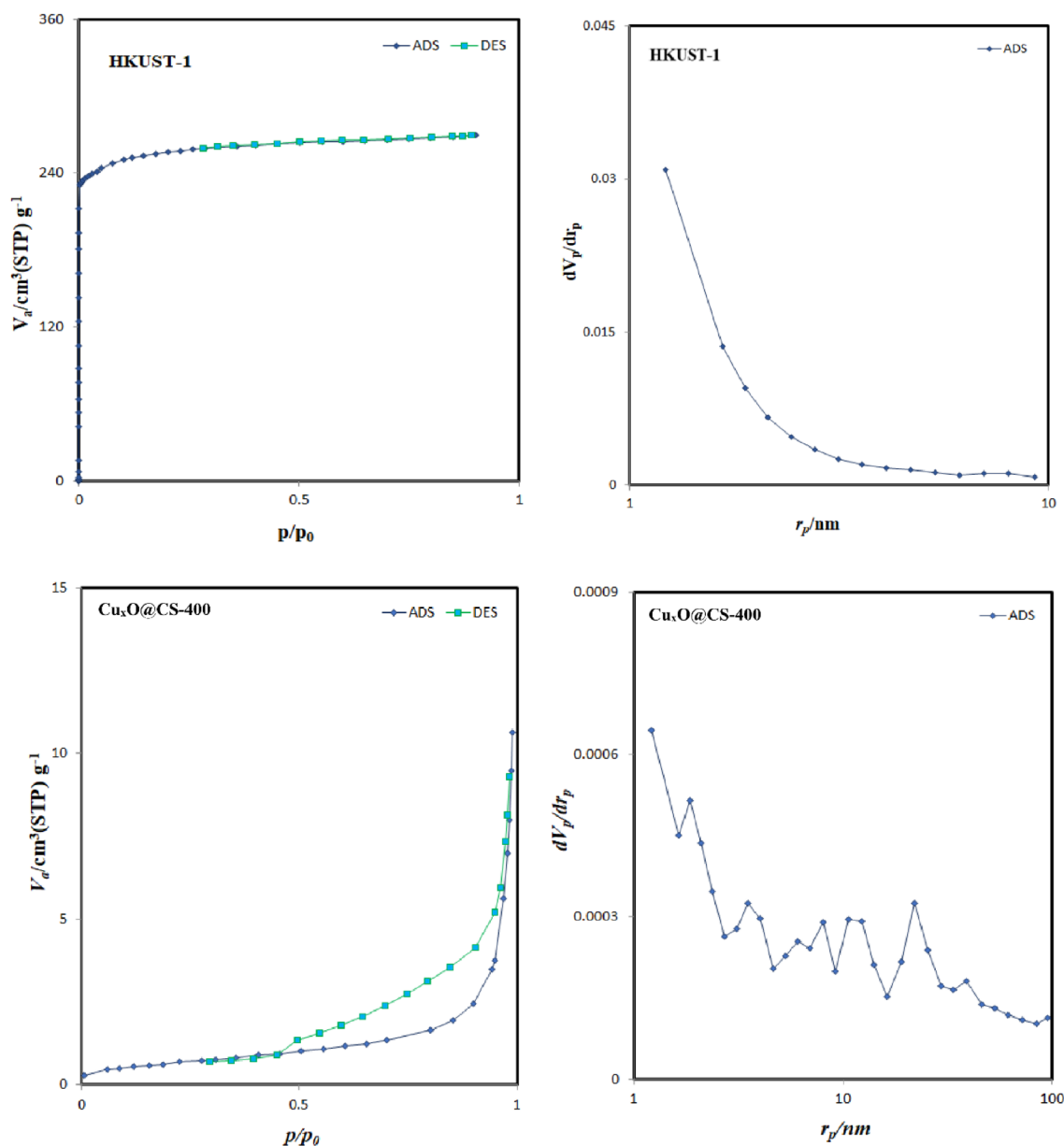


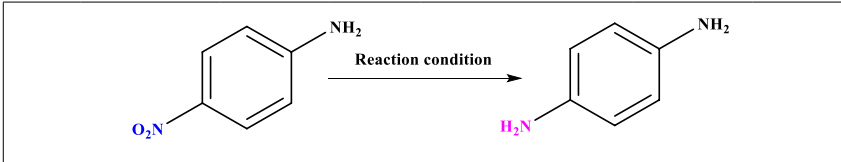
Figure 10. The N_2 adsorption–desorption isotherms of HKUST-1 and $Cu_xO@CS-400$ (H:D 1:2) catalyst.

Performance comparison of $Cu_xO@CS-400$ in hydrogenation of aromatic nitro compounds with other reported MOF-derived Cu-based catalysts

In this part of the research work, the catalytic efficiency and performance of $Cu_xO@CS-400$ in the hydrogenation reaction of nitroarenes were reconciled with the previously published MOF-derived Cu-based catalysts, and the outcomes are succinct in Table 3. However, every one of these catalysts shown in Table 3 has its own advantages. It is clear that the above catalyst has shown significant activity and efficiency due to reaction conditions such as short reaction time, green solvent (H_2O), low temperature, appropriate amount of reductant, recovery and reusability, as well as time and product yield.

Recyclability and stability of $Cu_xO@CS-400$

Considering the environmental and economic advantages and the reusable characteristics of a catalyst, it is very important for economic and industrial applications. Accordingly, the reusability of $Cu_xO@CS-400$, under optimal reaction conditions was examined for the transformation of 4-nitroaniline to 1,4-phenylenediamine. The reaction vessel was supplemented with a fresh sample of 4-nitroaniline and the repurposed catalyst. When the reaction mix was stirred under ideal circumstances, 90% yield was produced after eight cycles, suggesting that $Cu_xO@CS-400$ could be recycled for the reduction of 4-nitro aniline (Fig. 12). After the eight cycles, the product formation efficiency decreased to 86%, which could be due to copper oxide leaching. So, atomic absorption



Entry	Catalyst (mg)	Solvent	Temp °C	Reducing agent (equiv.)	Time (min)	Yield (%) ^b
1	None	H ₂ O	55	NaBH ₄ (2)	25	–
2	CS-400	H ₂ O	55	NaBH ₄ (2)	25	–
3	HKUST-1	H ₂ O	55	NaBH ₄ (2)	25	49
4	Cu _x O@C-400	H ₂ O	55	NaBH ₄ (2)	45	55
5	Cu _x O@CS-400 (3.5)	H ₂ O	55	NaBH ₄ (2)	28	100
6	Cu _x O@CS-400 (7)	H₂O	55	NaBH₄ (2)	20	100
7	Cu _x O@CS-400 (14)	H ₂ O	55	NaBH ₄ (2)	13	100
8	Cu _x O@CS-400 (7)	H ₂ O/EtOH	55	NaBH ₄ (2)	5	100
9	Cu _x O@CS-400 (7)	MeOH	55	NaBH ₄ (2)	20	95
10	Cu _x O@CS-400 (7)	Toluene	55	NaBH ₄ (2)	20	trace
11	Cu _x O@CS-400 (7)	THF		NaBH ₄ (2)	20	54
12	Cu _x O@CS-400 (7)	H ₂ O	75	NaBH ₄ (2)	10	100
13	Cu _x O@CS-400 (7)	H ₂ O	55	NaBH ₄ (1)	31	100
14	Cu _x O@CS-400 (7)	H ₂ O	55	NaBH ₄ (3)	15	100
15	Cu _x O@CS-400 (7)	H ₂ O	55	N ₂ H ₄ , H ₂ O (2)	70	98
16	Cu _x O@CS-400 (7)	H ₂ O	55	N ₂ H ₄ , H ₂ O (3)	62	98

Table 2. Reduction of 4-nitro aniline in different conditions^a. ^aReaction condition: 4-nitro aniline (1 mmol), NaBH₄, Solvent (3 mL), catalyst. ^bIsolated yield. E.g. Significant values are in [bold].

spectroscopy was performed on recycled catalyst and the percentage of copper was determined to be 64.1%, which indicates 1.4% decrease compared to the fresh catalyst.

To prove the stability and high activity of the Cu_xO@CS-400 catalyst, several stages of recovery were done, and finally, the structural characteristics and morphology of the recovered catalyst were compared with those of the fresh catalyst by accomplishing XRD and TEM analysis following the reusability examination (Fig. 13). This analysis indicated that the morphology of the Cu_xO@CS-400 catalyst used was relatively similar to the catalyst without recovery, which proves and confirms that it is a powerful catalyst (Fig. 13).

Conclusion

In conclusion, a sulfur doped HKUST-1 material was subjected to pyrolysis at 400 °C in a nitrogen atmosphere, resulting in the creation of an exquisite heterogeneous nano-catalyst. This novel heterogeneous catalyst, named Cu_xO@CS-400, underwent comprehensive characterization and exhibited outstanding performance in the reduction reaction of nitro aromatic compounds. It also demonstrated excellent recovery capability, with a yield of 90% over eight consecutive cycles. Furthermore, even after the eighth cycle, Cu_xO@CS-400 keeps its original morphology, indicating its long-lasting nature. The catalyst offers several advantages, including its simple synthesis, short reaction time, eco-fraternal disposition, thermal resistance, and remarkable catalytic activity and reusability. These attributes make Cu_xO@CS-400 a highly desirable catalyst for various catalytic applications.

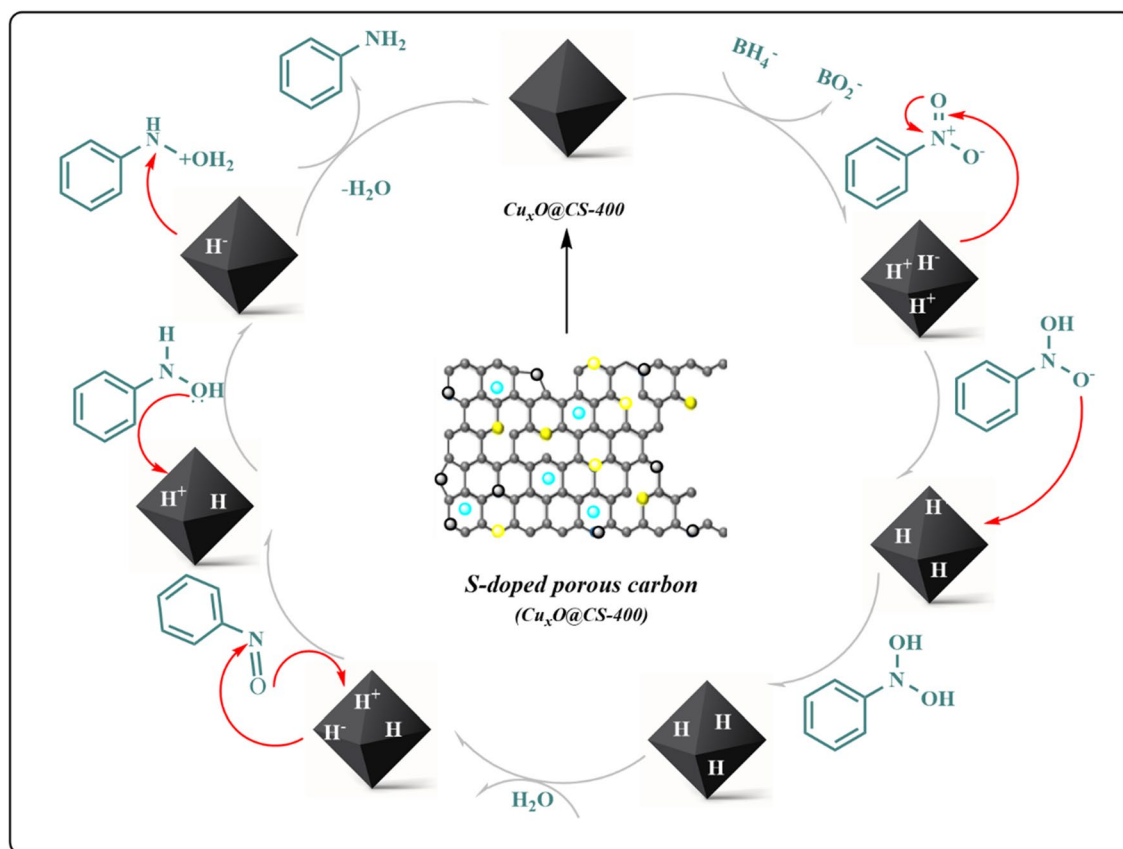


Figure 11. Mechanistic sight for the hydrogenation of the nitroarenes by $\text{Cu}_x\text{O@CS-400}$.

Entry	Catalyst	Reaction conditions	Time (h)	Yield (%)	Refs.
1	$\text{Cu}_x\text{O@CS-400}$ 7 mg	4-Nitro aniline (1 mmol), NaBH_4 (2 mmol), H_2O (3 mL), 55 °C	20 min	100	This article
2	Cu@C-400 15 mg	Nitrobenzene (2 mmol), EtOH (10 mL), NaBH_4 (4 mmol, added in two times), 45 °C	30 min	100	⁵⁰
3	$\text{Cu/Cu}_2\text{O/C}$ 0.04 mg	4-Nitrophenol (5×10^{-3} M), NaBH_4 (0.2 M), H_2O (2 mL), RT	2.67 min	99	⁵¹
4	$\text{Cu/Cu}_2\text{O@C}$ 10 mg	4-Nitroaniline, NaBH_4 (0.1M), H_2O , RT	1	100	⁵²
5	$\text{Cu/Cu}_2\text{O@C-rGO}$ 1 mg	4-Nitrophenol (0.3×10^{-3} mmol), NaBH_4 (0.25 mmol), H_2O (2 mL), RT	90	98	⁵³
6	a- Cu@C 5 mol %	Nitrobenzene (1 mmol), THF/ H_2O (1:2. 3 mL), NaBH_4 (3 mmol), 50 °C	4	98	⁵⁴

Table 3. Checking the catalytic power of $\text{Cu}_x\text{O@CS-400}$ with some MOF-derived Cu-based catalysts in the reduction reaction of para-nitro aniline.

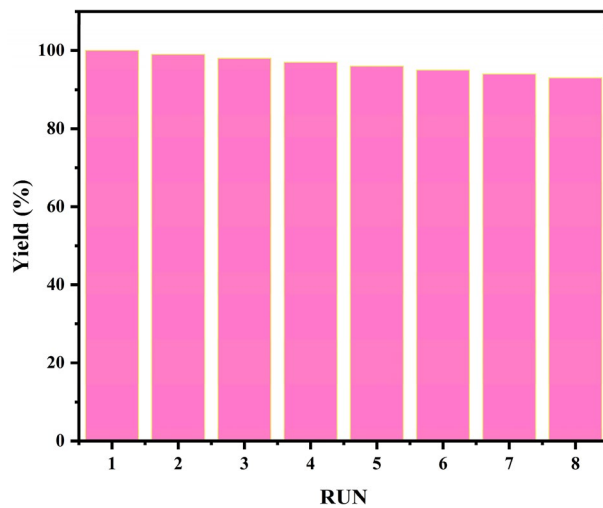


Figure 12. The recycling of the CuO_x@CS-400 catalyst.

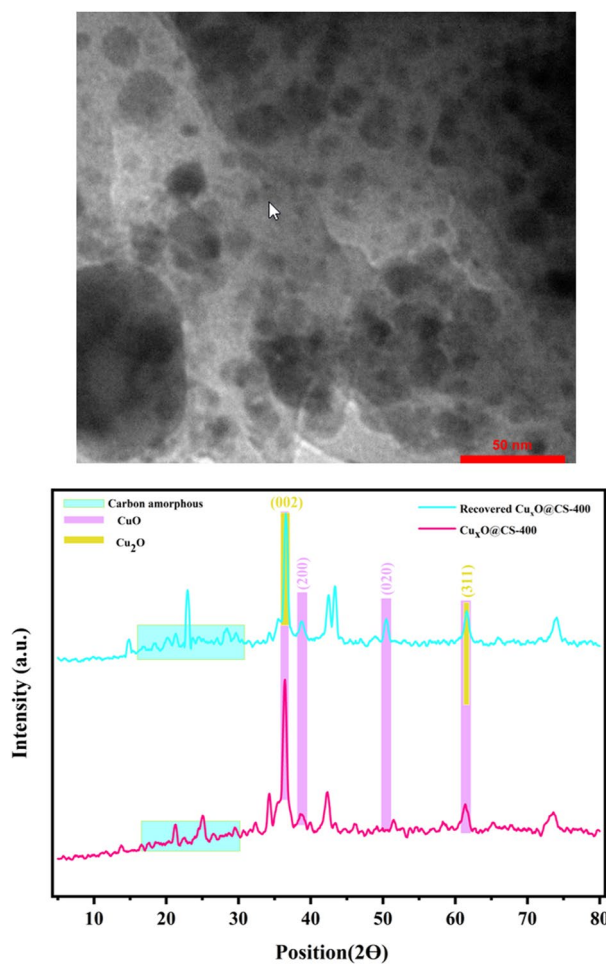


Figure 13. TEM image and XRD patterns of fresh and recovered Cu_xO@CS-400 after the 8th cycle.

Data availability

All data generated or analyzed during this study are included in this published article.

Received: 8 December 2023; Accepted: 21 February 2024

Published online: 06 March 2024

References

- Nanadegani, Z. S., Nemati, F., Elhampour, A. & Rangraz, Y. Cobalt oxide NPs immobilized on environmentally benign biological macromolecule-derived N-doped mesoporous carbon as an efficient catalyst for hydrogenation of nitroarenes. *J. Solid State Chem.* **292**, 121645. <https://doi.org/10.1016/j.jssc.2020.121645> (2020).
- Salimifar, B., Nemati, F. & Elhampour, A. PANI-g-C₃N₄ grafted on cobalt acetate as an efficient precursor for synthesis of N-doped carbon contains cobalt composite: A versatile catalyst for reduction of nitro compounds. *Diam. Relat. Mater.* **103**, 107695. <https://doi.org/10.1016/j.diamond.2020.107695> (2020).
- Ren, J. *et al.* Recent progress on MOF-derived carbon materials for energy storage. *Carbon Energy* **2**, 176–202. <https://doi.org/10.1002/cey2.44> (2020).
- Chen, W. *et al.* Preparation of nitrogen and sulfur dual-doped mesoporous carbon for supercapacitor electrodes with long cycle stability. *Electrochim. Acta* **177**, 327–334. <https://doi.org/10.1016/j.electacta.2015.01.093> (2015).
- Wu, Y., Wang, L., Chen, L., Li, Y. & Shen, K. Morphology-engineering construction of anti-aggregated Co/N-doped hollow carbon from metal-organic frameworks for efficient biomass upgrading. *Small* <https://doi.org/10.1002/sml.202207689> (2023).
- Sridhar, V., Lee, I. & Park, H. Metal organic frameworks derived Fe-NC nanostructures as high-performance electrodes for sodium ion batteries and electromagnetic interference (EMI) shielding. *Molecules* **26**, 1018. <https://doi.org/10.3390/molecules26041018> (2021).
- Han, A. *et al.* Recent advances for MOF-derived carbon-supported single-atom catalysts. *Small Methods* **3**, 1800471. <https://doi.org/10.1002/smt.201800471> (2019).
- Van Nguyen, C., Lee, S., Chung, Y. G., Chiang, W.-H. & Wu, K.C.-W. Synergistic effect of metal-organic framework-derived boron and nitrogen heteroatom-doped three-dimensional porous carbons for precious-metal-free catalytic reduction of nitroarenes. *Appl. Catal. B Environ.* **257**, 117888. <https://doi.org/10.1016/j.apcatb.2019.117888> (2019).
- Zhang, Q. *et al.* Preparation of heteroatom-doped carbon materials and applications in selective hydrogenation. *ChemistrySelect* **7**, e202102581. <https://doi.org/10.1002/slct.202102581> (2022).
- Chattopadhyay, J., Pathak, T. S. & Pak, D. Heteroatom-doped metal-free carbon nanomaterials as potential electrocatalysts. *Molecules* **27**, 670. <https://doi.org/10.3390/molecules27030670> (2022).
- Wang, J., Wang, Y., Hu, H., Yang, Q. & Cai, J. From metal-organic frameworks to porous carbon materials: Recent progress and prospects from energy and environmental perspectives. *Nanoscale* **12**, 4238–4268. <https://doi.org/10.1039/C9NR09697C> (2020).
- Chen, X., Xie, Y., Shao, Y., Shen, K. & Li, Y. Facile synthesis of boron and nitrogen dual-doped hollow mesoporous carbons for efficient reduction of 4-nitrophenol. *ACS Appl. Mater. Interfaces* **13**, 42598–42604. <https://doi.org/10.1021/acscami.1c08187> (2021).
- Gutru, R. *et al.* Recent progress in heteroatom doped carbon based electrocatalysts for oxygen reduction reaction in anion exchange membrane fuel cells. *Int. J. Hydrog. Energy* **48**, 3593–3631. <https://doi.org/10.1016/j.ijhydene.2022.10.177> (2023).
- Zhang, M. *et al.* Functional polymers-assisted confined pyrolysis strategy to transform MOF into hierarchical Co/N-doped carbon for peroxymonosulfate advanced oxidation processes. *Sep. Purif. Technol.* **305**, 122407. <https://doi.org/10.1016/j.seppur.2022.122407> (2023).
- Konnerth, H. *et al.* Metal-organic framework (MOF)-derived catalysts for fine chemical production. *Coord. Chem. Rev.* **416**, 213319. <https://doi.org/10.1016/j.ccr.2020.213319> (2020).
- Lu, Q., Eid, K. & Li, W. Heteroatom-doped porous carbon-based nanostructures for electrochemical CO₂ reduction. *Nanomaterials* **12**, 2379. <https://doi.org/10.3390/nano12142379> (2022).
- Chen, X. *et al.* MOF-derived isolated Fe atoms implanted in N-doped 3D hierarchical carbon as an efficient ORR electrocatalyst in both alkaline and acidic media. *ACS Appl. Mater. Interfaces* **11**, 25976–25985. <https://doi.org/10.1021/acscami.9b07436> (2019).
- Fu, Y. A., Huang, Y., Xiang, Z., Liu, G. & Cao, D. Phosphorous-nitrogen-codoped carbon materials derived from metal-organic frameworks as efficient electrocatalysts for oxygen reduction reactions. *Eur. J. Inorg. Chem.* **2016**, 2100–2105. <https://doi.org/10.1002/ejic.201500822> (2016).
- Wang, Y. *et al.* Degradation of norfloxacin by MOF-derived lamellar carbon nanocomposites based on microwave-driven Fenton reaction: Improved Fe (III)/Fe (II) cycle. *Chemosphere* **293**, 133614. <https://doi.org/10.1016/j.chemosphere.2022.133614> (2022).
- Peng, Y. *et al.* Applications of metal-organic framework-derived N, P, S doped materials in electrochemical energy conversion and storage. *Coord. Chem. Rev.* **466**, 214602. <https://doi.org/10.1016/j.ccr.2022.214602> (2022).
- Zhu, J., He, G., Tian, Z., Liang, L. & Shen, P. K. Facile synthesis of boron and nitrogen-dual-doped graphene sheets anchored platinum nanoparticles for oxygen reduction reaction. *Electrochim. Acta* **194**, 276–282. <https://doi.org/10.1016/j.electacta.2016.01.222> (2016).
- Yan, X. *et al.* Metal-organic framework (MOF)-derived catalysts for chemoselective hydrogenation of nitroarenes. *New J. Chem.* **45**, 18268–18276. <https://doi.org/10.1039/D1NJ03227E> (2021).
- Cao, J., Zhou, H., Huang, C., Wu, Q. & Yao, W. ZIF-8-derived Zn, N-codoped porous carbon as a high-performance piezocatalyst for organic pollutant degradation and hydrogen production. *J. Colloid Interface Sci.* **645**, 794–805. <https://doi.org/10.1016/j.jcis.2023.04.117> (2023).
- Mondol, M. M. H., Kim, C.-U. & Jhung, S. H. Titanium nitride@ nitrogen-enriched porous carbon derived from metal-organic frameworks and melamine: A remarkable oxidative catalyst to remove indoles from fuel. *J. Chem. Eng.* **450**, 138411. <https://doi.org/10.1016/j.cej.2022.138411> (2022).
- Ren, Q., Wang, H., Lu, X. F., Tong, Y. X. & Li, G. R. Recent progress on MOF-derived heteroatom-doped carbon-based electrocatalysts for oxygen reduction reaction. *Adv. Sci.* **5**, 1700515. <https://doi.org/10.1002/adv.201700515> (2018).
- Chen, W. *et al.* Heteroatom-doped carbon materials: synthesis, mechanism, and application for sodium-ion batteries. *Small Methods* **3**, 1800323. <https://doi.org/10.1002/smt.201800323> (2019).
- Yang, S., Peng, L., Bulut, S. & Queen, W. L. Recent advances of MOFs and MOF-derived materials in thermally driven organic transformations. *Chem. Eur. J.* **25**, 2161–2178. <https://doi.org/10.1002/chem.201803157> (2019).
- Zhan, F. *et al.* Metal-organic framework-derived heteroatom-doped nanoarchitectures for electrochemical energy storage: Recent advances and future perspectives. *Energy Storage Mater.* **52**, 685–735. <https://doi.org/10.1016/j.ensm.2022.08.035> (2022).
- Shaheen Shah, S., Abu Nayem, S., Sultana, N., Saleh Ahammad, A. & Abdul Aziz, M. Preparation of sulfur-doped carbon for supercapacitor applications: A review. *ChemSusChem* **15**, e202101282. <https://doi.org/10.1002/cssc.202101282> (2022).
- Oliveira, R. L. *et al.* Porous heteroatom-doped carbons: Efficient catalysts for selective oxidation of alcohols by activated persulfate. *ChemCatChem* **14**, e202200787. <https://doi.org/10.1002/cctc.202200787> (2022).
- Nakatsuka, K., Yoshii, T., Kuwahara, Y., Mori, K. & Yamashita, H. Controlled pyrolysis of Ni-MOF-74 as a promising precursor for the creation of highly active Ni nanocatalysts in size-selective hydrogenation. *Chem. Eur. J.* **24**, 898–905. <https://doi.org/10.1002/chem.201704341> (2018).

32. Su, T.-Y., Lu, G.-P., Sun, K.-K., Zhang, M. & Cai, C. ZIF-derived metal/N-doped porous carbon nanocomposites: Efficient catalysts for organic transformations. *Catal. Sci. Technol.* **12**, 2106–2121. <https://doi.org/10.1039/D1CY02211C> (2022).
33. Xu, S. *et al.* Multidimensional MOF-derived carbon nanomaterials for multifunctional applications. *J. Mater. Chem. A* <https://doi.org/10.1039/D3TA00239J> (2023).
34. Liu, W. *et al.* MOF-derived B, N co-doped porous carbons as metal-free catalysts for highly efficient nitro aromatics reduction. *J. Environ. Chem. Eng.* **9**, 105689 (2021).
35. Alhumaimess, M. S. Metal–organic frameworks and their catalytic applications. *J. Saudi Chem. Soc.* **24**, 461–473. <https://doi.org/10.1016/j.jscs.2020.04.002> (2020).
36. Shen, Y., Bao, L.-W., Sun, F.-Z. & Hu, T.-L. A novel Cu-nanowire@ Quasi-MOF via mild pyrolysis of a bimetal-MOF for the selective oxidation of benzyl alcohol in air. *Mater. Chem. Front.* **3**, 2363–2373. <https://doi.org/10.1039/C9QM00277D> (2019).
37. Xue, W. *et al.* Metal–organic frameworks-derived heteroatom-doped carbon electrocatalysts for oxygen reduction reaction. *Nano Energy* **86**, 106073. <https://doi.org/10.1016/j.nanoen.2021.106073> (2021).
38. Delmo, E. P. *et al.* Metal organic framework-ionic liquid hybrid catalysts for the selective electrochemical reduction of CO₂ to CH₄. *Chin. J. Catal.* **43**, 1687–1696. [https://doi.org/10.1016/S1872-2067\(21\)63970-0](https://doi.org/10.1016/S1872-2067(21)63970-0) (2022).
39. Hu, L., Li, W., Wang, L. & Wang, B. Turning metal–organic frameworks into efficient single-atom catalysts via pyrolysis with a focus on oxygen reduction reaction catalysts. *Energy Chem.* **3**, 100056. <https://doi.org/10.1016/j.enchem.2021.100056> (2021).
40. Huang, B., Liu, Y., Huang, X. & Xie, Z. Multiple heteroatom-doped few-layer carbons for the electrochemical oxygen reduction reaction. *J. Mater. Chem. A* **6**, 22277–22286. <https://doi.org/10.1039/C8TA06743K> (2018).
41. Ji, Y., Du, J. & Chen, A. Review on heteroatom doping carbonaceous materials toward electrocatalytic carbon dioxide reduction. *Trans. Tianjin Univ.* <https://doi.org/10.1007/s12209-022-00332-z> (2022).
42. Liu, D. *et al.* Recent advances in MOF-derived carbon-based nanomaterials for environmental applications in adsorption and catalytic degradation. *Chem. Eng. J.* **427**, 131503. <https://doi.org/10.1016/j.cej.2021.131503> (2022).
43. Mirhosseini, M. S. & Nemati, F. Fe/N co-doped mesoporous carbon derived from cellulose-based ionic liquid as an efficient heterogeneous catalyst toward nitro aromatic compound reduction reaction. *Int. J. Biol. Macromol.* **175**, 432–442. <https://doi.org/10.1016/j.ijbiomac.2021.02.009> (2021).
44. Mirhosseini, M. S. & Nemati, F. Metal-free aerobic oxidation of benzyl alcohols over the selective N, P dual-doped hollow carbon sphere as the efficient and sustainable heterogeneous catalyst under mild reaction condition. *Microporous Mesoporous Mater.* **329**, 111514. <https://doi.org/10.1016/j.micromeso.2021.111514> (2022).
45. Piri, M., Heravi, M. M., Elhampour, A. & Nemati, F. Silver nanoparticles supported on P, Se-codoped g-C₃N₄ nanosheet as a novel heterogeneous catalyst for reduction of nitroaromatics to their corresponding amines. *J. Mol. Struct.* **1242**, 130646. <https://doi.org/10.1016/j.molstruc.2021.130646> (2021).
46. Kim, T.-H., Jung, C.-Y., Bose, R. & Yi, S.-C. Cobalt encapsulated in the nitrogen and sulfur co-doped carbon nanotube supported platinum for the oxygen reduction reaction catalyst. *Carbon* **139**, 656–665. <https://doi.org/10.1016/j.carbon.2018.07.031> (2018).
47. Chen, C. *et al.* Immobilization of a thiol-functionalized ionic liquid onto HKUST-1 through thiol compounds as the chemical bridge. *RSC Adv.* **6**, 54119–54128 (2016).
48. Gautam, S., Singhal, J., Lee, H. & Chae, K. Drug delivery of paracetamol by metal–organic frameworks (HKUST-1): Improvised synthesis and investigations. *Mater. Today Chem.* **23**, 100647. <https://doi.org/10.1016/j.mtchem.2021.100647> (2022).
49. Yang, Y., Xu, D., Wu, Q. & Diao, P. Cu₂O/CuO bilayered composite as a high-efficiency photocathode for photoelectrochemical hydrogen evolution reaction. *Sci. Rep.* **6**, 35158. <https://doi.org/10.1038/srep35158> (2016).
50. Qiao, C. *et al.* MOF-derived Cu-nanoparticle embedded in porous carbon for the efficient hydrogenation of nitroaromatic compounds. *Catal. Lett.* **150**, 3394–3401. <https://doi.org/10.1007/s10562-020-03244-6> (2020).
51. Niu, H., Liu, S., Cai, Y., Wu, F. & Zhao, X. MOF derived porous carbon supported Cu/Cu₂O composite as high performance non-noble catalyst. *Microporous Mesoporous Mater.* **219**, 48–53. <https://doi.org/10.1016/j.micromeso.2015.07.027> (2016).
52. Karahan, Ö., Biçer, E., Taşdemir, A., Yürüm, A. & Gürsel, S. A. Development of efficient copper-based MOF-derived catalysts for the reduction of aromatic nitro compounds. *Eur. J. Inorg. Chem.* **2018**, 1073–1079. <https://doi.org/10.1002/ejic.201701320> (2018).
53. Yang, K. *et al.* Monodisperse Cu/Cu₂O@C core-shell nanocomposite supported on rGO layers as an efficient catalyst derived from a Cu-based MOF/GO structure. *Nanoscale* **10**, 17647–17655. <https://doi.org/10.1039/C8NR04475A> (2018).
54. Nguyen-Sorenson, A. H. *et al.* Highly active copper catalyst obtained through rapid MOF decomposition. *Inorg. Chem. Fron.* **6**, 521–526. <https://doi.org/10.1039/C8QI01217B> (2019).

Acknowledgements

The authors gratefully acknowledge the Semnan University Research Council for the financial support of this work.

Author contributions

M.A.: did the experimental work and methodology. F. N.: Supervision, financial support, reviewing and editing the manuscript, and is the corresponding author of the manuscript. Z.E.: Write the first draft of the manuscript. Y. R.: Advisor, reviewing and editing the manuscript and is the secondary corresponding author of the manuscript.

Competing interests

The authors declare that they have no known competing financial interests or personal relationships that could have appeared to influence the work reported in this paper.

Additional information

Correspondence and requests for materials should be addressed to F.N.

Reprints and permissions information is available at www.nature.com/reprints.

Publisher's note Springer Nature remains neutral with regard to jurisdictional claims in published maps and institutional affiliations.



Open Access This article is licensed under a Creative Commons Attribution 4.0 International License, which permits use, sharing, adaptation, distribution and reproduction in any medium or format, as long as you give appropriate credit to the original author(s) and the source, provide a link to the Creative Commons licence, and indicate if changes were made. The images or other third party material in this article are included in the article's Creative Commons licence, unless indicated otherwise in a credit line to the material. If material is not included in the article's Creative Commons licence and your intended use is not permitted by statutory regulation or exceeds the permitted use, you will need to obtain permission directly from the copyright holder. To view a copy of this licence, visit <http://creativecommons.org/licenses/by/4.0/>.

© The Author(s) 2024